Journal of Asian Ceramic Societies 1 (2013) 17–25

Journal of Asian Ceramic Societies

Journal of Asian Ceramic Societies

journal homepage: www.elsevier.com/locate/jascer

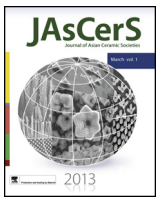

Review article

Recent development of sulfide solid electrolytes and interfacial modification for all-solid-state rechargeable lithium batteries

Masahiro Tatsumisago*, Motohiro Nagao, Akitoshi Hayashi

Department of Applied Chemistry, Graduate School of Engineering, Osaka Prefecture University, 1-1 Gakuen-cho, Naka-ku, Sakai, Osaka 599-8531, Japan

ARTICLE INFO

Article history:
Received 17 February 2013
Accepted 18 March 2013
Available online 9 April 2013

Keywords:
Sulfide solid electrolyte
Interfacial modification
All-solid-state battery
Rechargeable lithium battery

ABSTRACT

Recent development of inorganic sulfide solid electrolytes and all-solid-state rechargeable lithium batteries with them is reviewed. Electrical conductivity, electrochemical stability and chemical stability of these sulfide electrolytes are reported. Formation of favorable solid–solid contacts between electrode and electrolyte is important in all-solid-state batteries. Useful techniques to achieving intimate electrode–electrolyte interfaces are proposed. Application of sulfur positive electrode and lithium metal negative electrode with large theoretical capacity to all-solid-state lithium batteries is demonstrated.

Contents

1. Introduction

Increasing demands for high-power and high-energy rechargeable batteries have developed battery technology. Lithium-ion batteries consist of graphite negative electrode, organic liquid electrolyte, and lithium transition-metal oxide ($LiCoO_2$) positive electrode; these were firstly commercialized in 1991 and then such batteries have been widely spread out all over the world as a power source for mobile electronic devices such as cell phone, laptop and camcorder [1–3]. Nowadays, large-scale lithium ion batteries have been developed for application to automotive propulsion and stationary load-leveling for intermittent power generation from solar or wind energy. However, increasing battery size makes safety issues of lithium-ion batteries more serious; one reason is increasing amounts of flammable organic liquid electrolytes [4].

* Corresponding author. Tel.: +81 72 2549331; fax: +81 72 2549331.
E-mail addresses: tatsu@chem.osakafu-u.ac.jp (M. Tatsumisago), hayashi@chem.osakafu-u.ac.jp (A. Hayashi).

Peer review under responsibility of The Ceramic Society of Japan and the Korean Ceramic Society.

ELSEVIER Production and hosting by Elsevier

2187-0764 © 2013 The Ceramic Society of Japan and the Korean Ceramic Society. Production and hosting by Elsevier B.V. All rights reserved.
http://dx.doi.org/10.1016/j.jascer.2013.03.005

All-solid-state rechargeable lithium batteries have attracted much attention because the replacement of an organic liquid electrolyte with a safer and more reliable inorganic solid electrolyte (SE) simplifies the battery design and improves safety and durability of the battery [5–7]. Furthermore, direct stacking of solid-state cells in one package achieves a high operating voltage and reduces wasteful volume, and especially these features are favorable for vehicle application [8]. Another advantage of all-solid-state batteries is a possibility for use of fascinating large-capacity electrode materials, which are difficult to use in a conventional liquid electrolyte batteries. Lithium metal negative electrode and sulfur positive electrode are symbolic examples for the usage in all-solid-state batteries and will be demonstrated later.

A key material to develop all-solid-state batteries is a SE with high Li^+ ion conductivity at room temperature. Inorganic SEs have been widely studied and, in recent years, several SEs having the same level of conductivity as organic liquid electrolytes have been discovered [9,10]. Another key point is how to make a favorable solid–solid interface between electrode and electrolyte. Several techniques for increasing contact area at the interface have been developed to enhance utilization of active materials and rate capability.

In this paper, recent development of Li^+ ion conducting inorganic SEs is reviewed. Oxide and sulfide electrolytes have been widely studied, and these electrolytes are classified into three parts of crystal, glass, and glass–ceramic (crystallized glass). The conductivity and structure of typical electrolytes of oxides and sulfides are described. Electrochemical and chemical stability of sulfide electrolyte are also reported. A variety of active materials have been applied to all-solid-state rechargeable cells with sulfide electrolytes. The correlation of cell potential and cell capacity for the cells reported so far is summarized. Effective techniques to achieve favorable contacts between electrode and electrolyte developed by our group are proposed. Electrochemical performance of all-solid-state cells with sulfur positive electrode or lithium negative electrode is demonstrated.

2. Development of solid electrolytes

Solid materials as an electrolyte for battery application include a large variety of materials such as gel, organic polymer, organic–inorganic hybrids, and inorganic materials. In this report, we focus on inorganic SEs. Three categories are in inorganic electrolytes: crystalline, glass and glass–ceramic electrolytes. Oxide and sulfide compounds have been widely studied as inorganic electrolytes. The conductivity at 25 °C of typical oxide and sulfide SEs are listed in Table 1. The relationship between conductivity and structure is discussed in the following sections.

2.1. Crystalline electrolytes

In oxide electrolytes, crystalline phosphate with NASICON (*Na* Super *I*onic *Con*ductor)-type structures such as $Li_{1+x}Al_xTi_{2-x}(PO_4)_3$ (LATP) and $Li_{1+x}Al_xGe_{2-x}(PO_4)_3$ (LAGP) are known as excellent Li^+ ion conductors [11]. Perovskite $Li_{0.5-3x}La_{0.5+x}TiO_3$ (LLT) exhibits the high level of bulk conductivity of 10^{-3} S cm^{-1}, but total conductivity including grain-boundary resistance decreases by two orders of magnitude [12]. LATP and LLT electrolytes have Ti element in crystalline structure, and thus transition metal such as Ti is easily reduced by lithium metal negative electrode; it is thus difficult for these electrolytes to use in lithium metal batteries. Recently, garnet-type crystal $Li_7La_3Zr_2O_{12}$ (LLZ) has been attracting much attention because of its high conductivity of 3×10^{-4} S cm^{-1} and high chemical stability against lithium negative electrode [13]. All-solid-state rechargeable lithium metal batteries with the LLZ electrolyte showed a good cycleability [14]. Effective sintering to decrease grain boundary is important to increase total conductivity of those oxide crystalline electrolytes. An alternative idea is the use of glass–ceramic electrolytes. By crystallizing LATP or LAGP phase from a precursor glass, the effect of grain boundary resistance on total conductivity is highly reduced.

Sulfide SEs have a benefit of high conductivity of over 10^{-4} S cm^{-1} at room temperature. Another merit of sulfide electrolytes is easy reduction of grain-boundary resistance by conventional cold-press of electrolyte powders [15]; this mechanical property of sulfides is preferable for application to all-solid-state batteries. Sulfide crystals with a high conductivity of over 10^{-3} S cm^{-1} have been firstly reported by Kanno et al. [16]. A series of thio-LISICON (thio-*Li* Super *I*onic *Con*ductor) were synthesized and the solid-solution of $Li_{3.25}Ge_{0.25}P_{0.75}S_4$ showed a high conductivity of 2.2×10^{-3} S cm^{-1}. Argyrodite-type crystals Li_6PS_5X (X = Cl, Br, I) also have a high conductivity of over 10^{-3} S cm^{-1} [17]. Very recently, it has been found that $Li_{10}GeP_2S_{12}$ with a different crystal structure from the thio-LISICON phase has a higher conductivity of 1.2×10^{-2} S cm^{-1} [10]. Organic liquid electrolytes in commercially available lithium-ion batteries have a conductivity of 10^{-2} S cm^{-1}. However, the lithium ion transference number of a liquid electrolyte is less than 0.5 because anion species as well as lithium cations are mobile. It is noteworthy that the sulfide crystalline electrolytes with higher lithium-ion conductivity than a liquid electrolyte have been successfully prepared.

2.2. Glass electrolytes

Most oxide glass electrolytes show a low conductivity at room temperature, but some glasses with high Li^+ ion concentration such as lithium ortho-oxosalts have a relatively high ion conductivity of 10^{-6} S cm^{-1} [18,19]. LiPON (*Li*thium *P*hosphorous *Oxy*n*i*tride) amorphous thin-film also has the same level of conductivity [20]. LiPON has been used in thin-film batteries because reducing the electrolyte thickness decreases its resistance.

Sulfide glasses with high Li^+ ion concentration show high conductivity. In the system Li_2S–P_2S_5, the glasses with Li_2S more than 70 mol% have a conductivity of over 10^{-4} S cm^{-1} [21]. In general, it is difficult to prepare sulfide glasses with higher Li^+ ion concentration because of easy crystallization during cooling process. Thus the glasses are prepared by twin-roller rapid-quenching or mechanical milling techniques. The combination of two anion species is effective in increasing conductivity of glasses, and this effect is called as "mixed-anion effect" [18]. The addition of lithium salts is useful for enhancing conductivity of glasses because of the increase in lithium concentration and the decrease in activation energy for conduction. The lithium salts such as lithium halides [22], lithium borohydride ($LiBH_4$) [23] and lithium ortho-oxosalts (Li_3PO_4) [24] were added to sulfide glasses and the conductivity increased from the order of 10^{-4} to 10^{-3} S cm^{-1} at room temperature.

2.3. Glass–ceramic electrolytes

Crystallization of glass electrolytes produces glass–ceramic (crystallized glass) electrolytes. Precipitation of thermodynamically stable crystalline phases from a precursor glass is useful for reducing grain-boundary resistance; grain-boundaries among crystal domains are filled with amorphous phases and thus LATP and LAGP glass–ceramics showed a high conductivity [25,26]. On the other hand, a superionic conducting crystal is often precipitated by crystallization of glasses. A high-temperature phase or metastable phase tends to be crystallized as a primary phase from a supercooled liquid beyond glass transition temperature. In the

Table 1
Conductivity at 25 °C of oxide and sulfide solid electrolytes for all-solid-state lithium batteries.

Composition	Conductivity at 25 °C (S cm^{-1})	Classification	Reference
$Li_{1.3}Al_{0.3}Ti_{1.7}(PO_4)_3$	7×10^{-4}	Crystal (NASICON)	Aono et al. [11]
$La_{0.51}Li_{0.34}TiO_{2.94}$	1.4×10^{-3}	Crystal (perovskite)	Ito et al. [12]
$Li_7La_3Zr_2O_{12}$	3×10^{-4}	Crystal (garnet)	Murugan et al. [13]
$50Li_4SiO_4{\cdot}50Li_3BO_3$	4.0×10^{-6}	Glass	Tatsumisago et al. [18]
$Li_{2.9}PO_{3.3}N_{0.46}$	3.3×10^{-6}	Amorphous (thin film)	Yu et al. [20]
$Li_{3.6}Si_{0.6}P_{0.4}O_4$	5.0×10^{-6}	Amorphous (thin film)	Kanehori et al. [19]
$Li_{1.07}Al_{0.69}Ti_{1.46}(PO_4)_3$	1.3×10^{-3}	Glass–ceramic	Fu et al. [25,26]
$Li_{1.5}Al_{0.5}Ge_{1.5}(PO_4)_3$	4.0×10^{-4}	Glass–ceramic	Fu et al. [25,26]
$Li_{10}GeP_2S_{12}$	1.2×10^{-2}	Crystal	Kamaya et al. [10]
$Li_{3.25}Ge_{0.25}P_{0.75}S_4$	2.2×10^{-3}	Crystal	Kanno et al. [16]
Li_6PS_5Cl	1.3×10^{-3}	Crystal (argyrodite)	Boulineau et al. [17]
$30Li_2S{\cdot}26B_2S_3{\cdot}44LiI$	1.7×10^{-3}	Glass	Wada et al. [22]
$50Li_2S{\cdot}17P_2S_5{\cdot}33LiBH_4$	1.6×10^{-3}	Glass	Yamauchi et al. [23]
$63Li_2S{\cdot}36SiS_2{\cdot}1Li_3PO_4$	1.5×10^{-3}	Glass	Aotani et al. [24]
$70Li_2S{\cdot}30P_2S_5$	1.6×10^{-4}	Glass	Zhang et al. [21]
$Li_7P_3S_{11}$	1.1×10^{-2}	Glass–ceramic	Seino et al. [31]
$Li_{3.25}P_{0.95}S_4$	1.3×10^{-3}	Glass–ceramic	Mizuno et al. [27]

system Li_2S–P_2S_5, $Li_7P_3S_{11}$ or $Li_{3.25}P_{0.95}S_4$ was crystallized from the glasses at the compositions of 70 mol% or 80 mol% of Li_2S, respectively and the prepared glass–ceramics showed high conductivities of over 10^{-3} S cm^{-1} [27,28].

A typical example is the precipitation of a $Li_7P_3S_{11}$ high-temperature phase from the precursor glass. Fig. 1 shows (a) a differential thermal analysis (DTA) curve, (b) X-ray diffraction (XRD) patterns and (c) temperature dependence of conductivities for the $70Li_2S{\cdot}30P_2S_5$ (mol%) glass and glass–ceramics. The DTA curve of the glass shows an endothermic change of glass transition phenomena at 210 °C (T_g) and several exothermic peaks attributable to crystallization over T_g. The glass–ceramics were prepared by heating the glass up to the temperatures indicated by arrows in Fig. 1(a), and their XRD patterns are shown in Fig. 1(b). The $Li_7P_3S_{11}$ phase is precipitated as a primary phase by heating the glass at 240 °C and the crystallinity of $Li_7P_3S_{11}$ increases by heating at 360 °C. After heating at 550 °C, $Li_7P_3S_{11}$ completely disappears and thermodynamically stable phases such as $Li_4P_2S_6$ appear. As shown in Fig. 1(c), the conductivity increases by heating the glass at 240 or 360 °C, while the conductivity decreases by heating at 550 °C. The conductivity depends on the precipitated crystalline phases. The precipitation of the $Li_4P_2S_6$ phase with a low conductivity of 10^{-6} S cm^{-1} decreases the conductivity of glass–ceramic prepared at 550 °C. On the other hand, the $Li_7P_3S_{11}$ phase increases the conductivity and decreases the activation energy for conduction; the highest conductivity of 3.2×10^{-3} S cm^{-1} and the lowest activation energy of 12 kJ mol^{-1} are obtained for the glass–ceramic prepared at 360 °C. The $Li_7P_3S_{11}$ crystal was also directly precipitated by quenching the melt (kept at 700 °C), suggesting that $Li_7P_3S_{11}$ is a high-temperature phase [29]. The crystal was not synthesized by a conventional solid-state reaction and only prepared by crystallization from the glass or melt at the composition $70Li_2S{\cdot}30P_2S_5$. Electronic conductivity of the glass–ceramic with $Li_7P_3S_{11}$ was three orders of magnitude lower than ionic conductivity, indicating that ion transference number is almost unity. Preparation conditions of glass–ceramic with $Li_7P_3S_{11}$ have been examined and higher conductivities of 5.4×10^{-3} S cm^{-1} (by our group [30]) and 1.1×10^{-2} S cm^{-1} (by Seino et al. [31]) have been

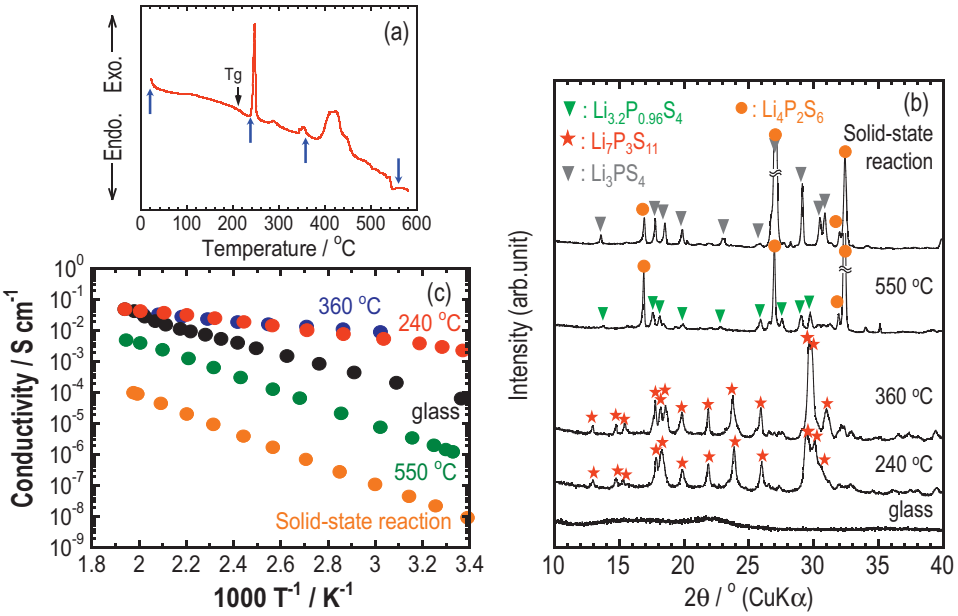

Fig. 1. (a) Differential thermal analysis (DTA) curve, (b) X-ray diffraction (XRD) patterns and (c) temperature dependence of conductivities for the $70Li_2S{\cdot}30P_2S_5$ (mol%) glass and glass–ceramics.

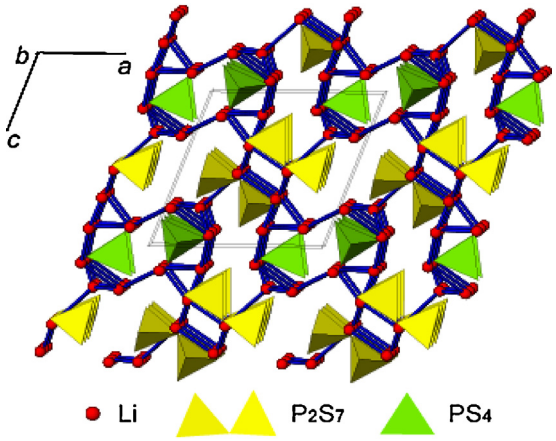

Fig. 2. Structural model of superionic $Li_7P_3S_{11}$ crystal.

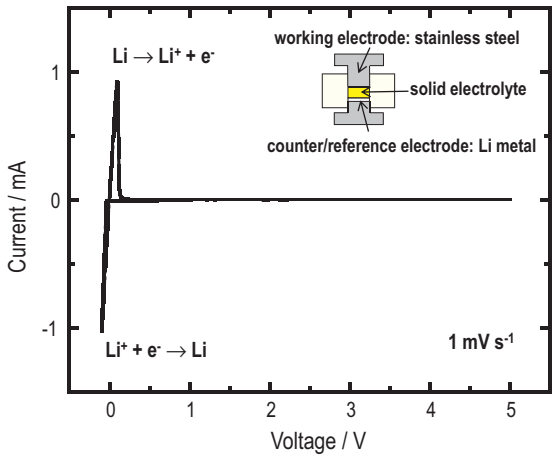

Fig. 3. Cyclic voltammogram of the $Li_7P_3S_{11}$ glass–ceramic electrolyte at the first cycle.

achieved at the present stage. Glass is a good precursor for yielding high-temperature phases, which usually exhibit much higher ionic conductivity than low-temperature phases. The crystallization of α-AgI [32] and cubic-Na_3PS_4 [15] from glassy state is also a typical example for developing SEs with high ion conductivity.

Fig. 2 shows the structural model of superionic $Li_7P_3S_{11}$ crystal [33]. The compound crystallizes in a triclinic cell, space group $P\bar{1}$, which were determined by using synchrotron X-ray powder diffraction pattern. Both PS_4^{3-} tetrahedral and $P_2S_7^{4-}$ ditetrahedral ions are contained in the structure and Li^+ ions are situated between them. The crystal structure is completely different from other superionic conducting crystals such as $Li_{3.25}Ge_{0.25}P_{0.75}S_4$ and $Li_{10}GeP_2S_{12}$, which are composed of only tetrahedral ions (PS_4^{3-} and GeS_4^{4-}). Li–Li correlations (solid blue lines) within 4 Å are illustrated in Fig. 2 and a favorable Li^+ conduction path is presumably close to the Li–Li chains. Recently, Li ion sites in $Li_7P_3S_{11}$ have been analyzed by neutron diffraction and Li^+ ion conduction pathway is discussed in detail [34,35].

2.4. Electrochemical window of sulfide electrolytes

Electrochemical window is also an important factor as SEs. Electrochemical stability of the $Li_7P_3S_{11}$ glass–ceramic electrolyte was examined by cyclic voltammetry. A stainless-steel disk as a working electrode and a lithium foil as a counter electrode were attached on each face of a pelletized electrolyte. The potential sweep was performed using a potentiostat/galvanostat device with a scanning rate of 1 mV s^{-1}. Cyclic voltammogram of the glass–ceramic at the first cycle is shown in Fig. 3. A cathodic current peak due to lithium deposition and an anodic current peak due to lithium dissolution are observed reversibly at around 0 V (vs. Li^+/Li). There is no large current peak except these peaks over the whole range from −0.1 V to 5.0 V. It is concluded that the glass–ceramic electrolyte has a wide electrochemical window of over 5 V and a good compatibility with lithium metal. The wide electrochemical window of 5 V was also observed for sulfide glasses with high conductivity of over 10^{-3} S cm^{-1}.

2.5. Chemical stability in air of sulfide electrolytes

Li_2S–P_2S_5 glasses and glass–ceramics have the advantage of a high lithium ion conductivity and a wide electrochemical window. The main drawback of these sulfide electrolytes is that they must be handled in an inert gas atmosphere since they have a low chemical stability in air. Hydrolysis of these sulfides by water molecules in air generates H_2S gas. The amounts of H_2S generated from Li_2S–P_2S_5 glasses were investigated [36]. Fig. 4 shows the amounts of H_2S generated from the pelletized Li_2S–P_2S_5 glasses with 67, 70, 75 and 80 mol% Li_2S, and Li_2S crystal. The measurement was done at room temperature under relative humidity of 48–51%. The amount of H_2S at the *y*-axis indicates the calculated amounts of H_2S generated by these sulfide samples after exposure to air for 1 min. The amount of H_2S decreased with increasing Li_2S content up to 75 mol% and the $75Li_2S{\cdot}25P_2S_5$ glass generated the smallest amount of H_2S (0.01 cm^3 g^{-1}) after exposure to air for 1 min. The amount of H_2S increased with a further increase in the Li_2S content. The Li_2S crystal generated a larger amount of H_2S than the $80Li_2S{\cdot}20P_2S_5$ glass. It is noteworthy that the amount of H_2S generated from the Li_2S–P_2S_5 glasses is extremely dependent on the glass composition. Furthermore chemical stability in air has been improved by partial substitution of oxides (Li_2O or P_2O_5) for sulfides (Li_2S or P_2S_5) [37,38]. An alternative approach to reduce H_2S generation is the addition of metal oxides which play a role in absorbing H_2S or bringing about acid–base reaction with H_2S. Metal oxides such as Fe_2O_3, ZnO and Bi_2O_3 have a largely negative value of Gibbs energy change (ΔG) for the following reaction: $M_xO_y + H_2S \rightarrow M_xS_y + H_2O$. The ball-milled composites of the $75Li_2S{\cdot}25P_2S_5$ glass and one of the metal oxides effectively suppressed the H_2S gas generation after the storage of the composites in air [39]. On the other hand, the $75Li_2S{\cdot}25P_2S_5$ glass did not generate H_2S gas under O_2 or N_2 gas flow with low humidity,

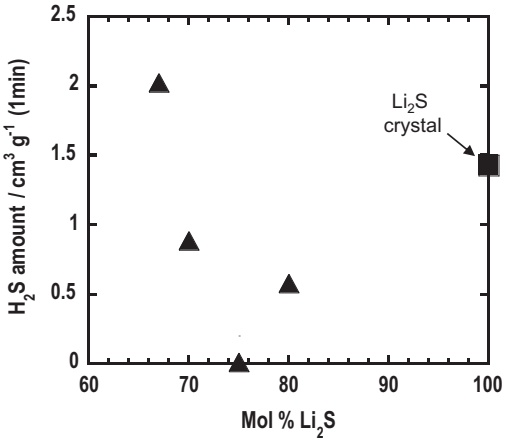

Fig. 4. H_2S amount generated from the pelletized Li_2S–P_2S_5 glasses and Li_2S crystal after exposed to air for 1 min.

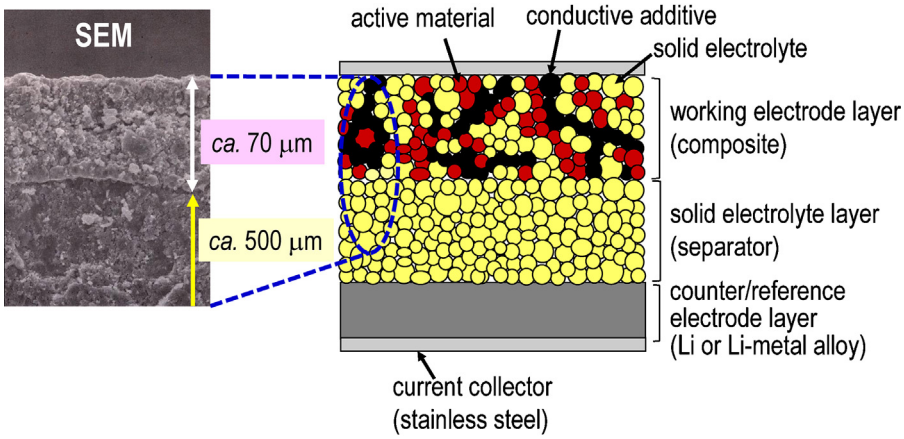

Fig. 5. Schematic of a typical all-solid-state electrochemical cell. Cross-sectional SEM image for the two layers of the working electrode and solid electrolyte (SE) is also shown.

suggesting that the sulfide glass has a good chemical stability in dry air atmosphere.

3. All-solid-state lithium rechargeable batteries

A bulk-type all-solid-state battery composed of compressed powder electrode/electrolyte layers has been studied. Compared to a thin film battery, a bulk-type battery attracts much attention because the battery is suitable for large-sized energy-storage devises. Li_2S-based sulfide materials as mentioned above are promising SE for bulk-type batteries. The electrochemical performance of all-solid-state cells with the Li_2S–SiS_2–Li_3PO_4 glasses was firstly reported by Iwamoto et al. [40] and then the cells with sulfide electrolytes have been developed. An intimate contact at the solid/solid interface between electrode and electrolyte is a key to improve battery performance. A schematic of a typical all-solid-state electrochemical cell is shown in Fig. 5. The cell consists of three layers. The first layer is Li–In alloy as a counter and/or reference electrode. The second layer is the Li_2S–P_2S_5 glass–ceramic powder as a SE. The third layer is a composite powder as a working electrode. In order to achieve smooth electrochemical reaction in the cell, the composite electrode composed of three kinds of particles is prepared; an active material ($LiCoO_2$), a SE, and a conductive additive (acetylene black, AB) particles with a weight ratio of 20:30:3 are mixed in order to form continuous lithium ion and electron conducting paths to $LiCoO_2$. Cross-sectional SEM image for the two layers of the working electrode and SE is also shown in Fig. 5. Obvious grain-boundary in the composite electrode and SE was not observed and intimate contacts between electrode and electrolyte were achieved by uniaxial cold-press. A typical thickness of working electrode and SE layers was ca. 70 μm and ca. 500 μm, respectively.

3.1. Preparation of all-solid-state batteries with sulfide electrolytes

A variety of active materials have been applied to bulk-type all-solid-state cells. Fig. 6 summarizes the correlation between cell potential (vs. Li^+/Li) and reversible capacity (per gram of active material) in all-solid-state cells with a sulfide SE reported so far. The active materials are classified into four categories on the basis of cell potential; (I) lithium transition-metal oxides and phosphates with a potential of 3.5–5 V (green circle), (II) sulfur-based materials with 2 V (yellow circle), (III) conversion-reaction materials with 1–2 V (blue circle), and (IV) alloying reaction materials with below 1 V (red circle).

The category (I) includes high-potential positive electrodes: $LiCoO_2$ [41,42], $LiNiO_2$ [43], $LiNi_{0.8}Co_{0.15}Al_{0.05}O_2$ [44], $LiNi_{0.33}Co_{0.33}Mn_{0.33}O_2$ [45], $LiMn_2O_4$ [46], $LiFePO_4$ [47] and $LiCoPO_4$ [48]. $LiCoO_2$ is widely studied as a model positive electrode, and the electrochemical reaction mechanism is based on Li^+ intercalation/deintercalation process:

$$LiCoO_2 \underset{\text{discharge}}{\overset{\text{Charge}}{\rightleftarrows}} Li_{1-x}CoO_2 + xLi^+ + xe^-$$

The cell with $LiCoO_2$ exhibited an excellent cycle performance of maintaining a reversible capacity of ca. 100 mAh g^{-1} for 700 cycles [42]. In this category, $LiNi_{0.8}Co_{0.15}Al_{0.05}O_2$ showed the highest capacity of ca. 150 mAh g^{-1}, while $LiCoPO_4$ exhibited the highest cell potential of 4.7 V vs. Li^+/Li.

The category (II) has sulfur-based positive electrodes: TiS_2 [40], amorphous TiS_3 [49], Mo_6S_8 [50,51], $LiVS_2$ [52] and composite electrodes of S–Cu [53,54], S–C [55,56], Li_2S–Cu [57] and Li_2S–C [58].

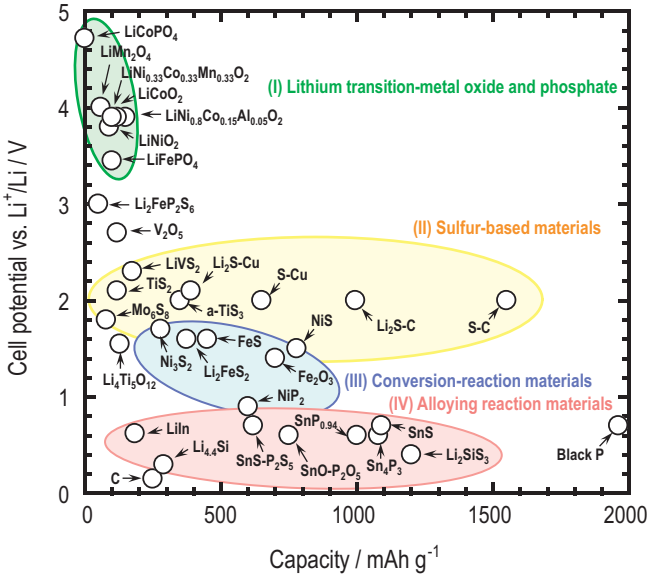

Fig. 6. Correlation between cell potential (vs. Li^+/Li) and reversible capacity (per gram of active material) in all-solid-state cells with a sulfide solid electrolyte reported so far.

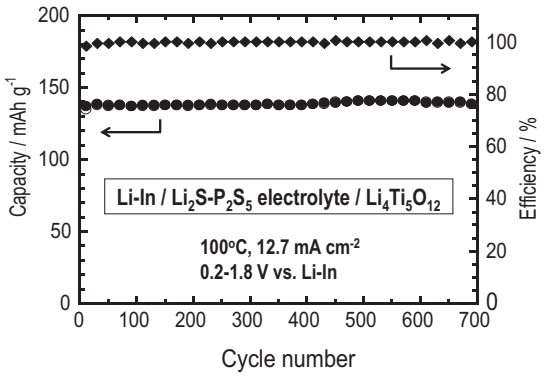

Fig. 7. Charge–discharge cycle performance of the all-solid-state Li–In/$Li_4Ti_5O_{12}$ cell. Open and solid circles respectively denote charge and discharge capacities and they overlap each other. Solid diamonds denote charge–discharge efficiency.

Layered-structure TiS_2 and Chevrel Mo_6S_8 are typical chalcogenide positive electrodes with high electronic conductivity and exhibit Li^+ intercalation/deintercalation process. The all-solid-state cell with Chevrel active materials operated as a secondary battery in the wide temperature range from −30 °C to 160 °C [51]. Amorphization of TiS_x is effective in increasing capacity and cycleability, and amorphous TiS_3 exhibited a higher capacity of 400 mAh g^{-1} than crystalline TiS_3 [49]. Sulfur and Li_2S (discharge product of sulfur) have a larger theoretical capacity than typical positive electrodes in the category (I). Because S and Li_2S are insulators, the addition of electronic conductivity by mixing with copper or nanocarbon is indispensable for the use of them. The electrochemical performance of S active material will be shown in Section 3.3.

The category (III) includes conversion-reaction electrodes: FeS [59], Li_2FeS_2 [60], Ni_3S_2 [61], NiS [62,63], NiP_2 [64] and Fe_2O_3 [65]. On behalf of the electrodes in this category, a reaction mechanism of NiS is as follows:

$$3NiS + 2Li^+ + 2e^- \rightleftarrows Ni_3S_2 + Li_2S$$

$$Ni_3S_2 + 4Li^+ + 4e^- \rightleftarrows 3Ni + 2Li_2S$$

(→: discharge, ←: charge)

The cell with NiS exhibited a large capacity of ca. 800 mAh g^{-1} with a good cycle performance. The electrodes in this category show a moderate potential of 1–2 V (vs. Li^+/Li) and thus these materials are applied as both positive and negative electrodes.

The category (IV) consists of electrodes forming lithium-alloy compounds: lithium alloys (LiIn [41] and $Li_{4.4}Si$ [66]), phosphides ($SnP_{0.94}$ [67] and Sn_4P_3 [68]), sulfides (SnS [69], Li_2SiS_3 [70] and SnS–P_2S_5 [69]) and an oxide (SnO–P_2O_5 [71]). These electrodes show a low potential with a large capacity and thus are used as a negative electrode. In particular, phosphides such as Sn_4P_3 or sulfides such as SnS–P_2S_5 are attractive because lithium-ion conducting phases (Li_3P or Li_2S–P_2S_5) are self-formed in the electrodes after electrochemical lithium insertion to those electrodes. As a low potential negative electrode, conventional graphite (carbon) [72] and black phosphorus [73] were used for all-solid-state cells. Black P with layered structure showed a quite large capacity of ca. 2000 mAh g^{-1} with a good cycleability; black P is a fascinating negative electrode for all-solid-state cells from the viewpoint of plentiful resource and large theoretical capacity.

Typical charge–discharge cycle performance of all-solid-state cells is shown in Fig. 7. $Li_4Ti_5O_{12}$ is a commercialized negative electrode and shows a moderate potential of 1.55 V (vs. Li^+/Li) as shown in Fig. 6 [42,74]. This electrode is a "zero-strain" material during charge–discharge processes and thus it is suitable for all-solid-state cells. The composite working electrode consisting of $Li_4Ti_5O_{12}$, Li_2S–P_2S_5 glass–ceramic SE, and vapor grown carbon fiber (VGCF) powders with a weight ratio of 38:58:4 was used for all-solid-state cells. The measurement was carried out under the constant current density of 12.7 mA cm^{-2} at 100 °C. The cell shows the discharge and charge capacity of about 140 mAh g^{-1} and maintains the capacity for 700 cycles with no degradation under a high current density of over 10 mA cm^{-2} [74]. All-solid-state cells essentially exhibit long cycle life. There are few reports about the high temperature operation of battery, and all-solid-state batteries using glass–ceramic electrolytes have a benefit of high temperature application.

3.2. Approaches to form electrode/electrolyte interface

Formation of favorable contacts at electrode–electrolyte solid–solid interfaces is a key to improve electrochemical performance of all-solid-state batteries because charge-transfer reaction proceeds only at the contact interfaces. Both the achievement of close contacts and the increase in contact areas are important to realize an effective charge-transfer reaction. A schematic of several approaches to form interfaces developed in our group is shown in Fig. 8.

An often-used approach to fabricate electrode–electrolyte contacts is the preparation of nanocomposites by a ball milling process [58,75]. A mixture of Li_2S active material, Li_2S–P_2S_5 SE, and acetylene black (AB, conductive additive) was ground with a high-energy planetary ball mill apparatus [58]. The secondary particles with a few micrometer in size were obtained as shown in SEM image. On the other hand, the cross-section of the particle was analyzed by STEM-EELS and the particle is a nanocomposite, where Li_2S (ca. 200 nm in size) and AB (ca. 100 nm in size) domains are dispersed and embedded in SE matrix. An all-solid-state cell with the Li_2S nanocomposite electrode exhibited a larger charge–discharge capacity and better cycleability than the cell with the Li_2S electrode prepared by hand-grinding of Li_2S, SE and AB.

Another approach is the surface coating of active material particles with SE thin films. Li_2S–P_2S_5 sulfide electrolyte thin films with the conductivity of ca. 10^{-4} S cm^{-1} on $LiCoO_2$ particles were prepared by a pulsed laser deposition (PLD) technique [76]. During deposition of the electrolyte, $LiCoO_2$ particles were fluidized by a vibrator in order to form the SE layer uniformly on them. The $LiCoO_2$ particles used in this study were coated with $LiNbO_3$ film in advance to suppress an interfacial resistance between $LiCoO_2$ and SE, achieving high-current drains in all-solid-state cells [77,78]. The cross-sectional TEM image shows the SE film with ca. 70 nm in thickness is formed with good adhesion to the surface of the $LiNbO_3$-coated $LiCoO_2$ particles. All-solid-state cells using only the SE-coated $LiCoO_2$ as a working electrode (without SE and AB particles) exhibited almost the same charge–discharge cycling performance of a typical cell using a working electrode prepared by mixing $LiCoO_2$ and SE particles. Therefore, the SE coating on active materials is an effective approach to increase energy density of all-solid-state cells.

The final approach is utilization of supercooled liquid of glass electrolyte. The mixture of active material and glass electrolyte is heated at around glass transition temperature of the electrolyte to fabricate solid–liquid interfaces [79]. After cooled down to room temperature, favorable electrode–electrolyte contacts are fabricated. Cross-section of pelletized mixture of $LiCoO_2$ and Li_2S–P_2S_5 glass was analyzed by SEM observation. After heat-treatment at 210 °C for 4 h, the SEM image suggests grain-boundaries and pores among $LiCoO_2$ particles were filled with softened glass domains, as compared to the SEM image before heat-treatment. An all-solid-state cell with the heat-treated $LiCoO_2$ electrode exhibited a larger

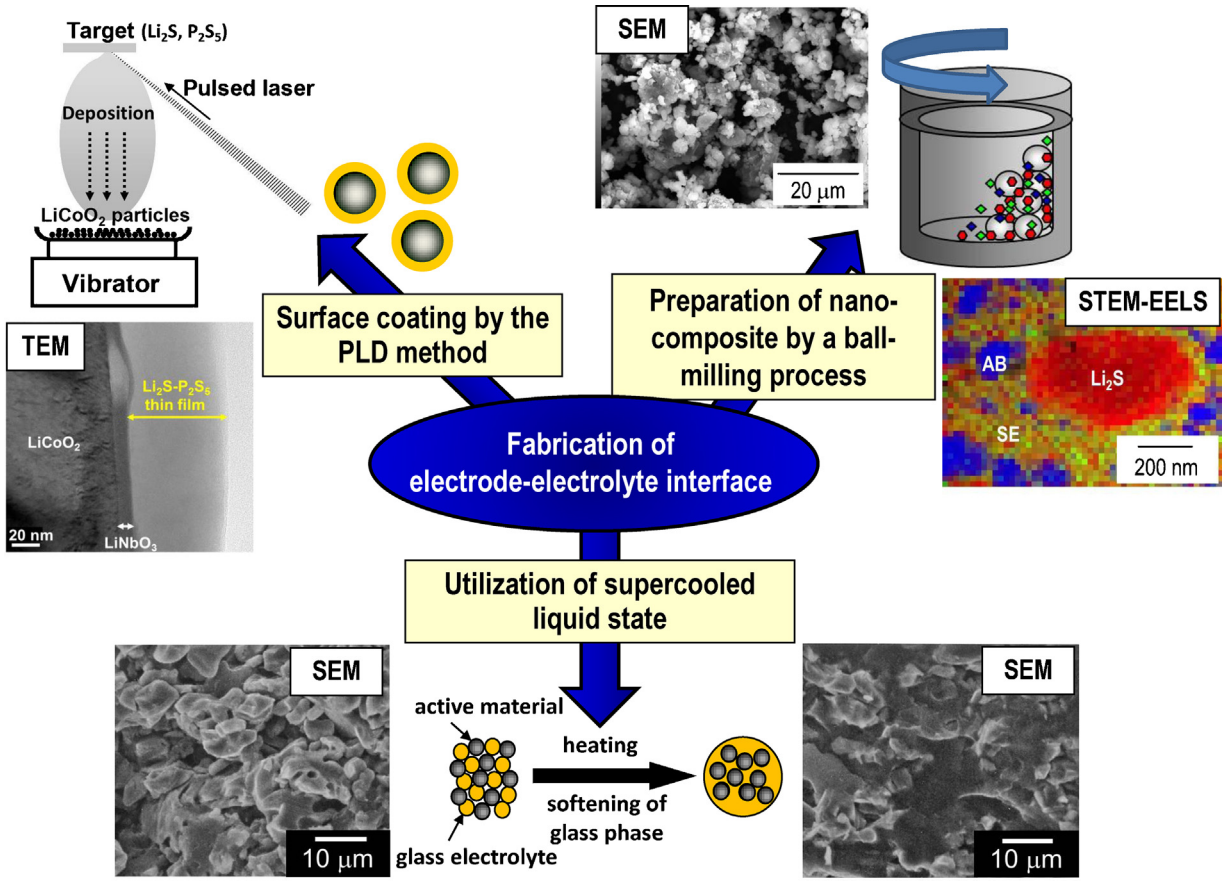

Fig. 8. Schematic of several approaches to form electrode/electrolyte interfaces developed in our group.

reversible capacity than a cell with the $LiCoO_2$ electrode without heat-treatment.

A favorable contact at the interface between electrode and electrolyte leads to a good performance of all-solid-state batteries. Formation techniques to give facile electrochemical reaction and enhance utilization of active materials should be developed for further improvement of battery performance.

3.3. Use of sulfur positive electrode

In order to improve energy density of all-solid-state batteries, the utilization of active materials with high capacity is effective. As just mentioned in category (II) in Fig. 6, elemental sulfur has been of great interest as a positive electrode material because of its large theoretical capacity of 1672 mAh g^{-1}, low cost, and environmental friendliness [80]. Unfortunately, the Li/S batteries with conventional liquid electrolytes suffer from rapid capacity fading on cycling because polysulfides formed during a discharge process dissolve in liquid electrolytes [81]. The use of inorganic SEs will resolve a key problem in Li/S batteries.

The composite electrode consisting of sulfur, Li_2S–P_2S_5 glass–ceramic SE, and AB powders with a weight ratio of 25:50:25 was prepared by high-energy planetary ball milling to form intimate contacts among the three components [56]. The charge–discharge curves of an all-solid-state Li–In/S cell at 25 °C under the current density of 0.064 mA cm^{-2} are shown in Fig. 9. Inset shows the cycle performance of the Li–In/S cell at a higher current density of 0.64 mA cm^{-2}. The cell exhibits a large reversible capacity of over 1500 mAh g^{-1} (of sulfur) with an average potential of ca. 2.1 V (vs. Li^+/Li). The charge–discharge curves of an all-solid-state cell with a typical positive electrode of $LiCoO_2$ are also shown in Fig. 9. The cell with sulfur electrode shows 15 times larger capacity than the cell with $LiCoO_2$, although an operating potential of the former cell is almost half of the latter cell; the sulfur cell has a considerably higher energy density than the $LiCoO_2$ cell. The sulfur cell retains about 1000 mAh g^{-1} for 200 cycles at 0.64 mA cm^{-2}. The cell operated in the wide temperature range from −20 to 80 °C.

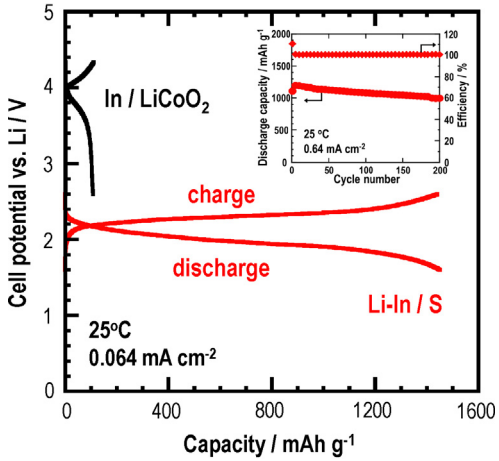

Fig. 9. Charge–discharge curves of an all-solid-state Li–In/S cell at 25 °C under the current density of 0.064 mA cm^{-2}. The curves for the cell with a typical positive electrode of $LiCoO_2$ are also shown for comparison. Inset shows the cycle performance of the Li–In/S cell at a higher current density of 0.64 mA cm^{-2}.

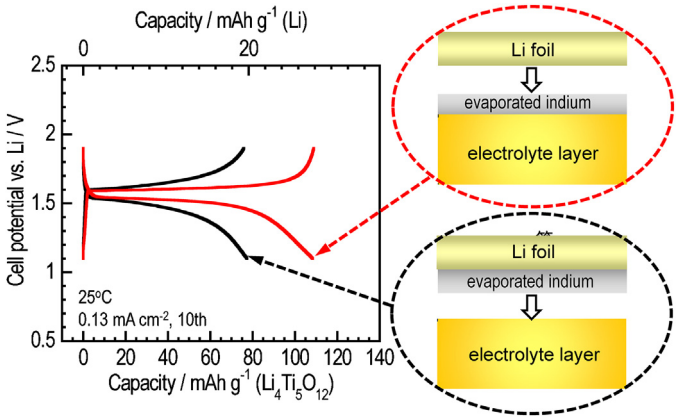

Fig. 10. Charge–discharge curves of the Li/SE/$Li_4Ti_5O_{12}$ cells at the 10th cycle under the current density of 0.13 mA cm^{-2} at 25 °C. An indium thin film was formed on the surface of solid electrolyte (SE) (red curve) or lithium foil (black curve).

On the other hand, lithium sulfide Li_2S, which is a reaction product after discharge for sulfur active material, was also used as a positive electrode with a large capacity in all-solid-state cells [58]; the merit of Li_2S instead of S is the compatibility with various negative electrodes without lithium sources such as graphite. Development of all-solid-state Li/S batteries will meet the demand of battery application with large energy density and long cycle life.

3.4. Use of lithium negative electrode

Rechargeable lithium metal battery is an ultimate energy storage system because lithium metal has an extremely high theoretical capacity (3860 mAh g^{-1}) and the lowest reaction potential among negative electrode materials [1]. However, lithium metal secondary batteries with a liquid electrolyte have not been practically used from the viewpoint of their safety and cycleability [82]. Suppression of dendritic growth of lithium metal during charge–discharge cycles is important and the use of inorganic SEs is useful for solving the issue. We have reported that a lithium or indium thin-film prepared by vacuum-evaporation was inserted at the interface between a Li_2S–P_2S_5 SE and a lithium electrode, and intimate contacts between them highly contributed to a reversibility of lithium dissolution and deposition in bulk-type all-solid-state cells [83,84].

Fig. 10 shows the charge–discharge curves of the Li/SE/$Li_4Ti_5O_{12}$ cells at the 10th cycle under the current density of 0.13 mA cm^{-2} at 25 °C. An indium thin film (with ca. 500 nm in thickness) was formed on the surface of SE (red curve) or lithium foil (black curve). The capacity based on the weight of $Li_4Ti_5O_{12}$ is shown on the lower horizontal-axis and that based on lithium is shown on the upper horizontal-axis in the figure. Both the cells using lithium electrode exhibit an average discharge potential of about 1.55 V, which coincides with the theoretical operating potential of $Li_4Ti_5O_{12}$ vs. lithium metal. It is confirmed that the insertion of the indium thin film does not change the operating potential of lithium metal cells. The cell prepared by evaporating indium on the SE layer (red curve) exhibits a higher capacity and a lower overpotential than that of the cell using indium evaporated on the lithium foil (black curve). This result suggests that the construction of a favorable interface between the indium thin film and the SE layer contributes to the enhancement of reversible capacity. The Li/$Li_4Ti_5O_{12}$ cells using the indium thin film were charged and discharged for 120 cycles. Inserting a lithium-alloy thin layer at the lithium–SE interface achieved a good cycleability because of continuous formation and retention of intimate contacts at the interface [84].

4. Conclusions

Development of inorganic sulfide SEs and their application to bulk-type all-solid-state rechargeable batteries are reviewed. Sulfide electrolytes have several advantages of high conductivity, single Li^+ ion conduction, wide electrochemical window and intimate solid/solid contact. In particular, $Li_{10}GeP_2S_{12}$ crystal and $Li_7P_3S_{11}$ glass–ceramic have a high conductivity over 10^{-2} S cm^{-1}, which is the same as the conductivity of an organic liquid electrolyte. Li_2S–P_2S_5 glass–ceramic electrolytes were used in all-solid-state batteries and the batteries exhibited excellent cycle performance. A possible use of active materials with large capacity such as sulfur and lithium metal, which are not available in conventional cells using a liquid electrolyte, is an advantage of all-solid-state batteries. Surface modification techniques using ball-milling, PLD-coating, and softening glass electrolytes are effective in forming intimate interface and enhancing contact areas between electrode and electrolyte.

Next issues to be solved for all-solid-state batteries are further increase of Li^+ ion conductivity and chemical stability of sulfide electrolytes, and the formation of electrode/electrolyte interface achieving rapid charge transfer. Control of size, morphology and dispersibility of both SE and active material particles are also important for achieving favorable solid/solid interface. Increasing amounts of active materials in a composite electrode layer is useful for increasing energy density and power density of all-solid-state batteries.

References

[1] J.-M. Tarascon and M. Armand, Nature, 414, 359–367 (2001).
[2] Y. Nishi, J. Power Sources, 100, 101–106 (2001).
[3] M. Armand and J.-M. Tarascon, Nature, 451, 652–657 (2008).
[4] W. Li, J.R. Dahn and D.S. Wainwright, Science, 264, 1115–1118 (1994).
[5] C. Julien and G.A. Nazri, Solid State Batteries: Materials Design and Optimization, Kluwer Academic Publishers, Boston (1994).
[6] T. Minami, M. Tatsumisago, M. Wakihara, C. Iwakura, S. Kohjiya and I.I. Tanaka, Solid State Ionics for Batteries, Springer-Verlag, Tokyo (2005).
[7] K. Takada, Acta Mater., 61, 759–770 (2013).
[8] Y. Kato, K. Kawamoto, R. Kanno and M. Hirayama, Electrochemistry, 80, 749–751 (2012).
[9] J.W. Fergus, J. Power Sources, 195, 4554–4569 (2010).
[10] N. Kamaya, K. Homma, Y. Yamakawa, M. Hirayama, R. Kanno, M. Yonemura, T. Kamiyama, Y. Kato, S. Hama, K. Kawamoto and A. Matsui, Nat. Mater., 10, 682–686 (2011).
[11] H. Aono, E. Sugimono, Y. Sadaoka, N. Imanaka and G. Adachi, J. Electrochem. Soc., 137, 1023–1027 (1990).
[12] M. Ito, Y. Inaguma, W.H. Jung, L. Chen and T. Nakamura, Solid State Ionics, 70/71, 203–207 (1994).
[13] R. Murugan, V. Thangadural and W. Weppner, Angew. Chem. Int. Ed., 46, 7778–7781 (2007).
[14] S. Ohta, T. Kobayashi, J. Seki and T. Asaoka, J. Power Sources, 202, 332–335 (2012).
[15] A. Hayashi, K. Noi, A. Sakuda and M. Tatsumisago, Nat. Commun., 3, 856 (2012).
[16] R. Kanno and M. Murayama, J. Electrochem. Soc., 148, A742–A746 (2001).
[17] S. Boulineau, M. Courty, J.-M. Tarascon and V. Viallet, Solid State Ionics, 221, 1–5 (2012).
[18] M. Tatsumisago, N. Machida and T. Minami, J. Ceram. Soc. Jpn., 95, 197–201 (1987).
[19] K. Kanehori, K. Matsumoto, K. Miyauchi and T. Kudo, Solid State Ionics, 9/10, 1445–1448 (1983).
[20] X. Yu, J.B. Bates, G.E. Jellison and F.X. Hart, J. Electrochem. Soc., 144, 524–532 (1997).
[21] Z. Zhang and J.H. Kennedy, Solid State Ionics, 38, 217–224 (1990).
[22] H. Wada, M. Menetrier, A. Levasseur and P. Hagenmuller, Mater. Res. Bull., 18, 189–193 (1983).
[23] A. Yamauchi, A. Sakuda, A. Hayashi and M. Tatsumisago, J. Power Sources, doi:10.1016/j.jpowsour.2012.12.001, in press
[24] N. Aotani, K. Iwamoto, K. Takada and S. Kondo, Solid State Ionics, 68, 35–39 (1994).
[25] J. Fu, Solid State Ionics, 96, 195–200 (1997).
[26] J. Fu, Solid State Ionics, 104, 191–194 (1997).
[27] F. Mizuno, A. Hayashi, K. Tadanaga and M. Tatsumisago, Solid State Ionics, 177, 2721–2725 (2006).

[28] F. Mizuno, A. Hayashi, K. Tadanaga and M. Tatsumisago, Adv. Mater., 17, 918–921 (2005).
[29] K. Minami, A. Hayashi and M. Tatsumisago, J. Ceram. Soc. Jpn., 118, 305–308 (2010).
[30] A. Hayashi, K. Minami, S. Ujiie and M. Tatsumisago, J. Non-Cryst. Solids, 356, 2670–2673 (2010).
[31] Y. Seino, T. Ota, T. Jyunke and K. Yanagi, Extend Abstracts of the 36th Symposium on Solid State Ionics in Japan, (2010) pp. 116–117.
[32] M. Tatsumisago, T. Saito and T. Minami, Chem. Lett., 790–791 (2001).
[33] H. Yamane, M. Shibata, Y. Shimane, T. Junke, Y. Seino, S. Adams, K. Minami, A. Hayashi and M. Tatsumisago, Solid State Ionics, 178, 1163–1167 (2007).
[34] Y. Onodera, K. Mori, T. Otomo, A.C. Hannon, S. Kohara, K. Itoh, M. Sugiyama and T. Fukunaga, J. Phys. Soc. Jpn., 79, (Suppl. A) 87–89 (2010).
[35] Y. Onodera, K. Mori, T. Otomo, M. Sugiyama and T. Fukunaga, J. Phys. Soc. Jpn., 81, 044802 (2012).
[36] H. Muramatsu, A. Hayashi, T. Ohtomo, S. Hama and M. Tatsumisago, Solid State Ionics, 182, 116–119 (2011).
[37] T. Ohtomo, A. Hayashi, M. Tatsumisago and K. Kawamoto, J. Non-Cryst. Solids, 364, 57–61 (2013).
[38] A. Hayashi, H. Muramatsu, T. Ohtomo, S. Hama and M. Tatsumisago, J. Alloys Compd., submitted for publication.
[39] A. Hayashi, H. Muramatsu, T. Ohtomo, S. Hama and M. Tatsumisago, J. Mater. Chem. A, accepted for publication.
[40] K. Iwamoto, N. Aotani, K. Takada and S. Kondo, Solid State Ionics, 70/71, 658–661 (1994).
[41] K. Takada, N. Aotani, K. Iwamoto and S. Kondo, Solid State Ionics, 86–88, 877–882 (1996).
[42] M. Tatsumisago and A. Hayashi, Funct. Mater. Lett., 1, 31–36 (2008).
[43] K. Takada, N. Aotani, K. Iwamoto and S. Kondo, Solid State Ionics, 79, 284–287 (1995).
[44] Y. Seino, T. Ota and K. Takada, J. Power Sources, 196, 6488–6492 (2011).
[45] H. Kitaura, A. Hayashi, K. Tadanaga and M. Tatsumisago, Electrochim. Acta, 55, 8821–8828 (2010).
[46] H. Kitaura, A. Hayashi, K. Tadanaga and M. Tatsumisago, Solid State Ionics, 192, 304–307 (2011).
[47] A. Sakuda, H. Kitaura, A. Hayashi, M. Tatsumisago, Y. Hosoda, T. Nagakane and A. Sakamoto, Chem. Lett., 41, 260–261 (2012).
[48] K. Tadanaga, F. Mizuno, A. Hayashi, T. Minami and M. Tatsumisago, Electrochemistry, 71, 1192–1195 (2003).
[49] A. Hayashi, T. Matsuyama, A. Sakuda and M. Tatsumisago, Chem. Lett., 41, 886–888 (2012).
[50] R. Kanno, M. Murayama, T. Inada, T. Kobayashi, K. Sakamoto, N. Sonoyama, A. Yamada and S. Kondo, Electrochem. Solid-State Lett., 7, A455–A458 (2004).
[51] M. Nagao, H. Kitaura, A. Hayashi and M. Tatsumisago, J. Electrochem. Soc., submitted for publication.
[52] K. Takada, T. Inada, A. Kajiyama, M. Kouguchi, S. Kondo and M. Watanabe, J. Power Sources, 97/98, 762–764 (2001).
[53] N. Machida, K. Kobayashi, Y. Nishikawa and T. Shigematsu, Solid State Ionics, 175, 247–250 (2004).
[54] A. Hayashi, T. Ohtomo, F. Mizuno, K. Tadanaga and M. Tatsumisago, Electrochem. Commun., 5, 701–705 (2003).
[55] T. Kobayashi, Y. Imada, D. Shishihara, K. Homma, M. Nagao, R. Watanabe, T. Yokoi, A. Yamada, R. Kanno and T. Tatsumi, J. Power Sources, 182, 621–625 (2008).
[56] M. Nagao, A. Hayashi and M. Tatsumisago, Electrochim. Acta, 56, 6055–6059 (2011).
[57] A. Hayashi, R. Ohtsubo and M. Tatsumisago, Solid State Ionics, 179, 1702–1705 (2008).
[58] M. Nagao, A. Hayashi and M. Tatsumisago, J. Mater. Chem., 22, 10015–10020 (2012).
[59] B.C. Kim, K. Takada, N. Ohta, Y. Seino, L. Zhang, H. Wada and T. Sasaki, Solid State Ionics, 176, 2383–2387 (2005).
[60] K. Takada, K. Iwamoto and S. Kondo, Solid State Ionics, 117, 273–276 (1999).
[61] T. Matsumura, K. Nakano, R. Kanno, A. Hirano, N. Imanishi and Y. Takeda, J. Power Sources, 174, 632–636 (2007).
[62] Y. Nishio, H. Kitaura, A. Hayashi and M. Tatsumisago, J. Power Sources, 189, 629–632 (2009).
[63] K. Aso, H. Kitaura, A. Hayashi and M. Tatsumisago, J. Mater. Chem., 21, 2987–2990 (2011).
[64] A. Hayashi, A. Inoue and M. Tatsumisago, J. Power Sources, 189, 669–671 (2009).
[65] H. Kitaura, K. Takahashi, F. Mizuno, A. Hayashi, K. Tadanaga and M. Tatsumisago, J. Electrochem. Soc., 154, A725–A729 (2007).
[66] R. Tamori, N. Machida and T. Shigematsu, J. Jpn. Soc. Powder Powder Metall., 48, 267–273 (2001).
[67] K. Aso, H. Kitaura, A. Hayashi and M. Tatsumisago, J. Ceram. Soc. Jpn., 118, 620–622 (2010).
[68] A. Ueda, M. Nagao, A. Inoue, A. Hayashi, Y. Seino, T. Ota and M. Tatsumisago, J. Power Sources, doi:10.1016/j.jpowsour.2013.01.061, in press
[69] A. Hayashi, T. Konishi, K. Tadanaga and M. Tatsumisago, Solid State Ionics, 177, 2737–2740 (2006).
[70] B.T. Hang, T. Ohnisi, M. Osada, X. Xu, K. Takada and T. Sasaki, J. Power Sources, 195, 3323–3327 (2010).
[71] A. Hayashi, T. Konishi, K. Tadanaga, T. Minami and M. Tatsumisago, Res. Chem. Intermed., 32, 497–506 (2006).
[72] Y. Seino, K. Takada, B.C. Kim, L. Zhang, N. Ohta, H. Wada, M. Osada and T. Sasaki, Solid State Ionics, 176, 2389–2393 (2005).
[73] M. Nagao, A. Hayashi and M. Tatsumisago, J. Power Sources, 196, 6902–6905 (2011).
[74] K. Minami, A. Hayashi, S. Ujiie and M. Tatsumisago, Solid State Ionics, 192, 122–125 (2011).
[75] A. Hayashi, Y. Nishio, H. Kitaura and M. Tatsumisago, Electrochem. Commun., 10, 1860–1863 (2008).
[76] A. Sakuda, A. Hayashi, T. Ohtomo, S. Hama and M. Tatsumisago, J. Power Sources, 196, 6735–6741 (2011).
[77] N. Ohta, K. Takada, Li. Zhang, R. Ma, M. Osada and T. Sasaki, Adv. Mater., 18, 2226–2229 (2006).
[78] N. Ohta, K. Takada, I. Sakaguchi, L. Zhang, R. Ma, K. Fukuda, M. Osada and T. Sasaki, Electrochem. Commun., 9, 1486–1490 (2007).
[79] H. Kitaura, A. Hayashi, T. Ohtomo, S. Hama and M. Tatsumisago, J. Mater. Chem., 21, 118–124 (2011).
[80] X. Ji and L.F. Nazar, J. Mater. Chem., 20, 9821–9826 (2010).
[81] D. Marmorstein, T.H. Yu, K.A. Striebel, F.R. McLarnon, J. Hou and E.J. Cairns, J. Power Sources, 89, 219–226 (2000).
[82] D. Aurbach, E. Zinigrad, Y. Cohen and H. Teller, Solid State Ionics, 148, 405–416 (2002).
[83] M. Nagao, A. Hayashi and M. Tatsumisago, Electrochem. Commun., 22, 177–180 (2012).
[84] M. Nagao, A. Hayashi and M. Tatsumisago, Electrochemistry, 80, 734–736 (2012).